Effect of polarizer dynamics on current-induced behaviors in magnetic nanopillars

Sergei Urazhdin, Weng Lee Lim, and Andrew Higgins
Department of Physics, West Virginia University, Morgantown, West Virginia 26506, USA
(Received 29 May 2009; revised manuscript received 14 July 2009; published 15 October 2009)

Magnetoelectronic nanodevices such as magnetic random access memory include two essential magnetic layers: a polarizing reference layer and a free layer whose configuration can be changed by spin-polarized current via spin-transfer effect. We present measurements of current-induced behaviors in nanodevices with fixed dimensions of the free layer, and varied dimensions of the polarizer. Current-induced precession occurs only at positive current for sufficiently thick polarizer, and only at negative current for thin polarizer, with an abrupt transition between these regimes. Bipolar current-induced precession was observed for a small range of extended polarizer thickness but the amplitude of precession in these devices is reduced. These behaviors are interpreted in terms of the coupling between magnetic layers caused by spin transfer. We suggest a device architecture utilizing the coupling for improved efficiency.

DOI: 10.1103/PhysRevB.80.144411 PACS number(s): 85.75.−d, 75.60.Jk, 75.70.Cn

I. INTRODUCTION

In magnetic random access memory, information is encoded by the magnetic configuration of a nanoscale "free" magnetic layer. Reading the bit amounts to detecting the magnetic configuration of the free layer, which is performed via giant or tunneling magnetoresistance. Writing is performed by applying current I, which switches the magnetic moment due to the spin-transfer torque effect (STT).[1] Although large magnetoresistance has been achieved in MgO tunnel junctions,[2] further development of magnetic memory has been impeded by the limitations of the writing process.

When nanomagnetic devices are subjected to a magnetic field H sufficient to destabilize all but one magnetic configuration, spin transfer causes precession of the free layer. The resulting oscillations of voltage across the device can be used for generation of microwaves with frequency tunable either by field or current, which can potentially find application in magnetic memory devices.[3] Precession at modest currents of less than 1 mA can be achieved by using sufficiently small/thin nanomagnets but their thermal fluctuations result in significant microwave linewidth broadening.[4] On the other hand, increasing the volume of nanomagnet results in an increase in power required for device operation.

Fast switching or precession at acceptably small input power will likely be achieved by utilizing advanced device architectures that optimize the efficiency of STT without compromising other aspects of performance. In this paper, we reexamine the role of the "fixed" reference magnetic layer utilized primarily to spin polarize the current. We propose a device architecture in which the efficiency of STT is enhanced by optimizing reference-layer geometry.

The effect of spin-polarized current on the free layer is described by the spin-transfer torque,[1]

$$\tau_F = \hbar I g_F \mathbf{s}_F \times (\mathbf{s}_F \times \mathbf{s}_R)/e, \quad (1)$$

where $\mathbf{s}_F(\mathbf{s}_R)$ is a unit vector parallel to the magnetization of the free layer (reference layer), positive current is defined to flow from the reference layer to the free layer, and the coefficient g_F is determined mostly by the polarizing properties of the reference layer and the angle between $\mathbf{s}_F$ and $\mathbf{s}_R$. The function g_F is positive in common magnetic structures consisting of Permalloy(Py)$=Ni_{80}Fe_{20}$ or CoFe magnetic layers separated by most metallic or insulating spacers. At positive current, the torque Eq. (1) causes a repulsion of $\mathbf{s}_F$ from $\mathbf{s}_R$, resulting in its switching into antiparallel configuration at small H or precession at sufficiently large H.

The reference layer also experiences a STT $\tau_R = -\hbar I g_R \mathbf{s}_R(\mathbf{s}_R \times \mathbf{s}_F)/e$ of magnitude similar to τ_F. In the most commonly used device geometry, this layer is made much thicker than the free layer to minimize the effects of STT. However, in practical implementations of magnetic memory devices, the reference layer will likely have similar dimensions to the free layer and its magnetic configuration will be determined by exchange biasing with an additional antiferromagnetic layer. In this geometry, the effects of STT on the reference layer are not always negligible.[5] We note that simultaneous effects of STT on two magnetic systems are not necessarily detrimental to current-induced behaviors. For instance, two magnetic point contacts located in proximity to each other can experience phase-locked precession induced by STT, resulting in narrowing of their microwave emission lines.[6,7]

In Sec. II, we present measurements exploring the effects of STT on the reference layer. We show that thickness and lateral dimensions of the reference layer have a significant effect on current-induced behaviors of nanomagnetic devices. All devices included Py reference layer and free layer. The free layer was patterned into elliptical nanopillar shape of thickness $t_F=5$ nm so that any differences among the device behaviors can be attributed to the different reference-layer geometries. We discuss three devices $P8$, $P5$, and $P2$ with reference layer of thicknesses $t_R=8$, 5, and 2 nm, respectively, patterned into the same dimensions as the free layer. We also studied devices $E4$, $E3$, and $E2$ with reference-layer thicknesses $t_R=4$, 3, and 2 nm, and lateral dimensions of several micrometers. We shall see below that devices with both geometries of reference layer exhibit the same overall dependence on t_R while the difference between their behaviors provides additional information about the origin of the observed spectroscopic features.

In Sec. III, we model the effects of reference-layer dimensions on current-induced behaviors and show that they are

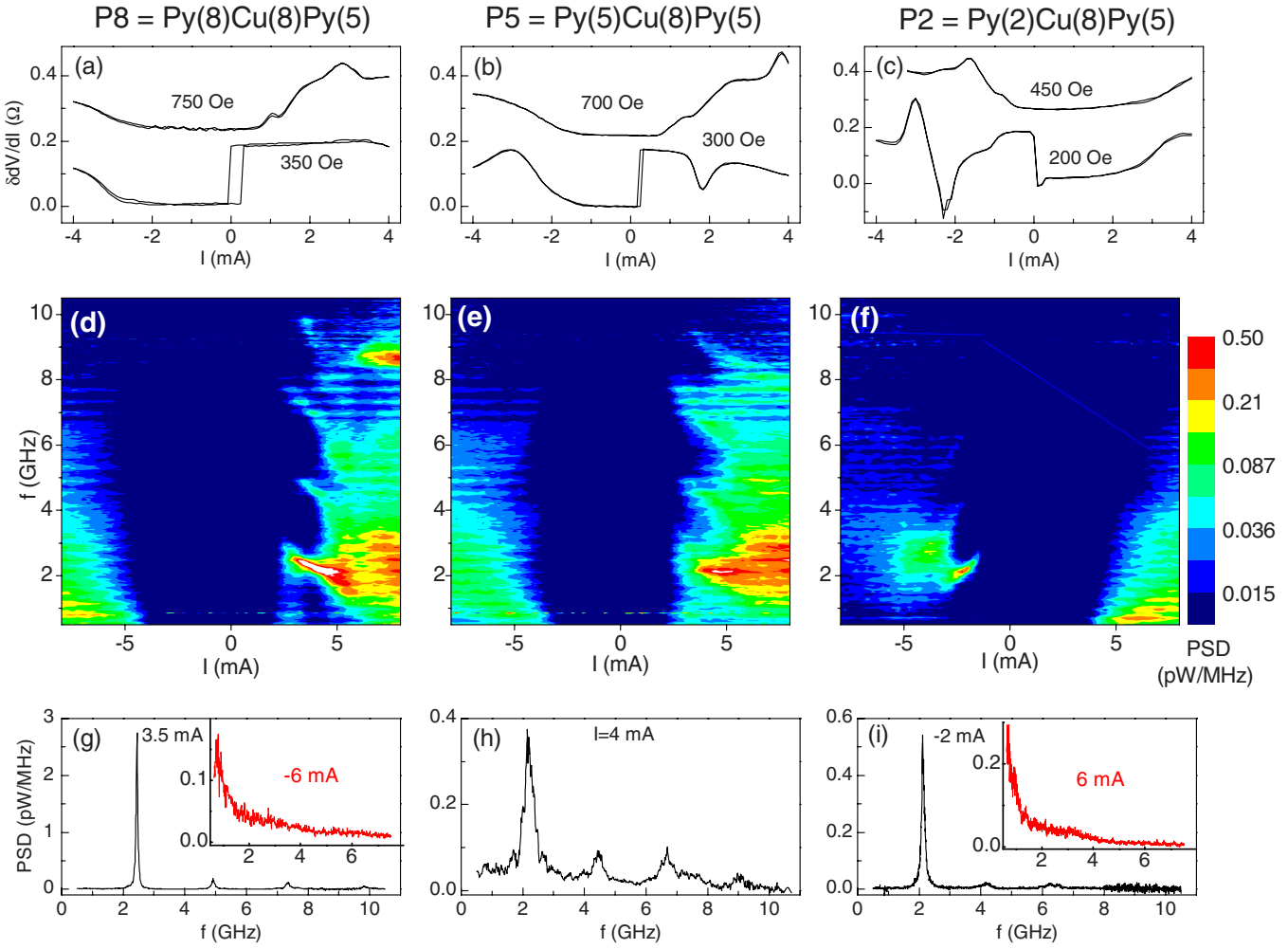

FIG. 1. (Color online) Data for devices with a patterned reference layer: $P8$ [(a), (d), and (g)], $P5$ [(b), (e), and (h)], and $P2$ [(c), (f), and (i)]. (a)–(c) dV/dI vs I at the labeled values of H. Curves are offset for clarity. (d)–(f) PSD at $H=750$ Oe, $H=700$ Oe, and $H=450$ Oe, respectively. (g)–(i) cross sections of (d)–(f), at the labeled values of I. The peaks are harmonically related.

caused by coupling between the layers induced by STT. We propose a device architecture utilizing this coupling to enhance the efficiency of spin transfer for microwave generation.

II. EXPERIMENTS

Multilayers Cu(50)Py(t_R)Cu(8)Py(5)Au(20), where Py $=Ni_{80}Fe_{20}$ and thicknesses are in nm, were deposited on oxidized silicon at 40 °C by magnetron sputtering at base pressure of 5×10^{-9} Torr, in 5 mTorr of purified Ar. The multilayers were patterned by Ar ion milling through an evaporated Al mask with dimensions of 100 nm$\times$50 nm. The milling was stopped in the middle of the Cu(8) spacer for devices with extended reference layer, and just below the bottom Py for devices with nanopatterned reference layer. We subsequently sputtered 30 nm of undoped Si without breaking the vacuum to electrically isolate the sample leads while avoiding device oxidation.[8] The mask was removed by a combination of ion milling with Ar beam nearly parallel to the sample surface, and 20 s etching in 1:10:1000 solution of $HNO_3:HF:H_20$, followed by sputtering of a 200-nm-thick Cu top contact.

The samples were contacted by microcoaxial probes, which were connected through a bias tee to a current source, a lock-in amplifier, and a spectrum analyzer through a 26 dB gain broadband amplifier. Differential resistance dV/dI was measured by superimposing an ac current of rms amplitude 20 μA on the dc current, with lock-in detection of the voltage. All measurements were performed at room temperature. The frequency-dependent gain of the amplifier, microwave losses in the cables, probes, and the sample leads were determined with a calibrated microwave generator and a power meter. The measured microwave signals were corrected for these gains/losses after subtracting the background determined from the spectra at $I=0$. The in-plane field $\mathbf{H}$ was rotated by 40° with respect to the nanopillar easy axis, unless specified otherwise.

The results for devices with nanopattered reference layer are summarized in Fig. 1. At small H in devices with reference layer much thicker than the free layer, negative current orients the free layer into the low-resistance parallel configuration with respect to the reference layer, and positive current

orients the free layer into the high-resistance antiparallel configuration. Devices *P*8 and *P*5 exhibited such switching characteristics [Figs. 1(a) and 1(b)]. In device *P*2, the switching occurred between antiparallel configuration at negative current and parallel configuration at positive current [Fig. 1(c)], indicating that the reference layer rather than the free layer was reversed by STT. Switching in all three devices is consistent with the stronger effects of STT on the smaller magnetic layer, resulting in its reversal before the effects of STT on the other layer become sufficient to cause its reversal. For *P*5, the switching of the free layer can be explained by the conical nanopillar shape obtained with our nanopatterning procedure, resulting in slightly larger lateral dimensions of the reference layer.

At larger H, switching was replaced by more gradual increases in dV/dI, which appeared for both polarities of current [Figs. 1(a)–1(c)]. In devices with reference layer much thicker than the free layer, such increases observed only at positive current are caused by the precession of the latter.[3] By extension, one can expect that the increases in dV/dI in our devices are caused by precession of the free layer at positive current and precession of the reference layer at negative current.[9] Indeed, spectroscopic measurements reveal bipolar excitations in all three devices [Figs. 1(d)–1(f)]. However, precession peaks appeared only at positive current in *P*8 and *P*5, and only at negative current in *P*2. Current in the opposite direction produced only broad $1/f$ noise [insets of Figs. 1(g) and 1(i)]. We attribute this noise to random thermal switching between the parallel and antiparallel magnetic configurations of the bilayer,[10] although its intensity is too small for unambiguous Lorentzian fitting. We shall see below that this noise is not present in devices with extended reference layer, consistently with the expected behaviors for a film exhibiting only a single stable magnetic configuration.

The emergence of the $1/f$ noise at positive current with reducing reference-layer thickness was correlated with an increased width of the precession peaks. The full width at half maximum (FWHM) of the first harmonic increased from the smallest value of 61 MHz at $I=3.5$ mA for *P*8, to 357 MHz at $I=4$ mA for sample *P*5 [Figs. 1(g) and 1(h)]. Precession peaks at positive current disappeared for *P*2 but the precession peaks that emerged at negative current exhibited the smallest FWHM of 117 MHz at $I=-2$ mA, smaller than for *P*5 at any current.

Broadening of the precession peaks is consistent with the increase in the $1/f$ background attributed to thermal telegraph noise. Expressing the power spectral density (PSD) of random telegraph noise through the average dwell times τ_P and τ_{AP} in parallel and antiparallel configurations,[11]

$$S(f) = 4\Delta V^2 \frac{(\tau_P \tau_{AP})^2}{(\tau_P + \tau_{AP})^3} \frac{f_c^2}{f_c^2 + 4\pi^2 f^2}, \tag{2}$$

where ΔV is the telegraph noise amplitude and $f_c = \tau_P^{-1} + \tau_{AP}^{-1}$ is the corner frequency. Assuming $f > f_c$ in the microwave frequency range, Eq. (2) gives power spectral density inversely proportional to the characteristic dwell times of the telegraph noise. On the other hand, τ_P sets the upper limit for the coherence time of precession, which determines the precession peak width. Therefore, the increase in $1/f$ noise simultaneously with broadening of the precession peaks is consistent with the effects of increasing telegraph noise rate.

The increase in the $1/f$ noise and the broadening of the precession peaks obscure another effect caused by the variations in the reference-layer thickness. Inspection of the spectroscopic data shows that precession of the free layer is suppressed in device *P*2 and precession of the reference layer is suppressed in device *P*8. In particular, the negative current data for *P*8 can be fitted with only a $1/f$ dependence [inset of Fig. 1(g)]. The positive current data for sample *P*2 [inset of Fig. 1(i) for $I=6$ mA] show a small peak with FWHM of 1.3 GHz centered at 3.1 GHz superimposed on the $1/f$ noise. However, the integrated power under this peak of 32 pW is only 8% of the total microwave power emitted by the device between 1 and 13.5 GHz.

Another signature of dynamics suppression can be seen in the increased dynamics onset currents determined either from the differential resistance or the spectroscopic data. The onset of precession or thermal switching causes a step or a peak in dV/dI.[12] From the dV/dI data in Figs. 1(a)–1(c), the onset of the free layer dynamics for *P*8 and *P*5 is $I_C^+ = 0.9$ mA, and 3 mA for *P*2. The onset of reference-layer dynamics is at $I_C^- = -0.4$ mA for *P*2, and −2 mA for *P*5 and *P*8. The dramatic increase in I_C^+ in *P*2, and of I_C^- in *P*5 and *P*8 is correlated with the suppression of precession peaks in spectroscopic measurements. Similar results are obtained from the analysis of spectroscopic data, as discussed below.

Extended magnetic films usually exhibit a single stable configuration. Consequently, our devices with extended layer more clearly show the suppression of precession not obscured by the $1/f$ noise. Figure 2 summarizes the results for these devices. At small field, the differential resistance for devices *E*4 and *E*3 showed the usual current-induced reversal of the free layer similar to other devices with thick reference layer [panels (a) and (b) in Fig. 2]. An extended reference layer cannot be reversed by STT that affects only the area of the point contact. Consequently, the switching behaviors did not reverse for a thin extended reference layer. Rather, current-induced switching did not occur in this device [panel (c)].

Spectroscopic results for positive current were similar to the devices with patterned reference layer. The FWHM of the precession peaks and the low-frequency background increased with decreasing t_R [panels (d) and (e)]. The precession peaks disappeared in *E*2 [panel (f)]. No dynamics were detected spectroscopically in *E*4 at negative current [panel (d)], and there were also no steps in the high-field dV/dI curves [400 Oe data in panel (a)]. In contrast, devices *E*3 and *E*2 exhibited precession peaks at negative current that were significantly narrower than for nanopatterned layers [panels (h) and (i)] but consistent with point contacts on extended magnetic layers.[13]

Summarizing the results for both types of devices, precession at negative current was suppressed for large t_R and precession at positive current was suppressed for small t_R. Among the data presented in Figs. 1 and 2 for six samples, only the device *E*3 exhibited clear bipolar precession. However, further analysis of spectroscopic data showed that precession of *both* layers was partly suppressed in *E*3. To quan-

titatively characterize the amplitude of the magnetic dynamics, we integrated the microwave power emitted by the devices between 1 and 13.5 GHz, and normalized it by the largest possible power emitted by a hypothetical oscillation between antiparallel and parallel configurations of the magnetic layers, $P_{max}=I^2\Delta R^2 R_L/8(R+R_L)^2$. Here, R is the time average of resistance and $R_L=50\ \Omega$ is the input impedance of the microwave amplifier. This formula was obtained by considering an equivalent circuit consisting of resistors $R \ll R_L$ connected in parallel to a source of dc current.

Two distinct spectroscopic features contribute to the microwave power emitted by the devices. The first feature is the $1/f$ noise that we attribute to random telegraph switching. The total power generated by the telegraph noise is dependent on its corner frequency, due to the low-frequency cutoff. The second contribution comes from the spectroscopic peaks and characterizes the precession amplitude. Ideally, these two contributions must be separately analyzed to quantitatively characterize the magnetic dynamics. In practice, the power is usually dominated by the precession whenever the precession peaks are clearly distinguishable, and it becomes impossible to separate the broad precession peaks from the $1/f$ noise when the latter dominates, for example, at $I>5$ mA in Fig. 1(d) for $P8$ or at $I<-2.5$ mA in Fig. 1(f) for $P2$. Therefore, we only analyze the total emitted power and separately comment on the two distinct contributions to it.

The integrated power emitted by both types of devices followed two distinct trends. Power exceeding $0.4P_{max}$ was attained at positive current in devices $P8$ and $E4$, and at negative current in devices $P2$ and $E2$, reaching $0.94P_{max}$ in $P2$ at $I=-2.5$ mA (Fig. 3). In contrast, the power emitted at negative current in devices $P8$ and $E4$, and at positive current in device $E2$ never exceeded $0.2P_{max}$. The largest power emitted by $P2$ at positive current was $0.3P_{max}$ at 6.5 mA. However, it was produced entirely by the $1/f$ noise [inset of Fig. 1(i)]. The relative power P/P_{max} emitted by $P5$ was nearly identical to that of $P8$, consistent with the similarity of their dynamical properties. For $E3$, the amplitude of the peaks at negative current is the largest among all the devices with extended reference layer but the emitted power does not exceed $0.07P_{max}$, due to the small linewidth. Meanwhile, the relative power emitted by this device at positive current is nearly identical to $P2$ and does not exceed $0.17P_{max}$.

The variations in the dynamical onset currents determined from the microwave power data in Fig. 3 are correlated with the suppression of precession. In devices with patterned polarizer, the onset currents are −0.9 and 3.5 mA for $P2$, −2.5 and 1.5 mA for $P3$, and −3.5 and 1.5 mA for $P8$. These values are consistent with the positions of the differential resistance steps discussed above [Figs. 1(a)–1(c)]. The dramatic increase in the positive dynamics onset current in $P2$ and negative onset current in $P5$ and $P8$ are correlated with suppression of precession peaks. A similar correlation is apparent in the microwave power data for devices with extended polarizer [Fig. 3(b)].

The total emitted power sets an upper limit for the amplitude of the precession. Therefore, the data for both types of devices in Fig. 3 unambiguously demonstrate suppression of free-layer precession in devices with thin reference layers, and suppression of thick reference-layer precession. The transition from precession of the free layer at positive current to precession of the reference layer at negative current occurs at $t_R=t_F=5$ nm in devices with a patterned reference layer. For devices with extended reference layer, the transition occurs at a smaller $t_R=3$ nm. In both types of devices, the critical value of t_R appears to be related to the effective magnetic precession volume. For point contacts, the effective precessing area likely extends beyond the physical contact dimensions so that the geometry of $E3$ can be considered approximately symmetric with respect to the precessing volumes of the magnetic layers.

The geometry and characteristics of precession in point contacts can depend on experimental parameters such as the value of current, as well as the direction and magnitude of field. In particular, theoretical analysis shows that a transition between a propagating cylindrical spin wave and a self-localized spin-wave bullet can occur when the magnetic field is rotated with respect to the sample plane.[14] One may therefore expect that the resulting variations in the effective precession volume will cause suppression of precession at positive or at negative current in the same device.

We were able to observe such behaviors in device $E2$ by rotating H in the film plane by 55° with respect to the nanopillar easy axis (Fig. 4). For $H=200$ and 400 Oe, the precession peaks appeared at negative current but precession at positive current was suppressed. In particular, the microwave power emitted between 1 and 13.5 GHz at $I=-5$ mA was 130 and 95 pW for these values of field while the power emitted at 5 mA was 65 and 55 pW, respectively. For $H=600$ Oe and $H=800$ Oe, precession peaks appeared at positive current but were suppressed at negative current. The microwave power emitted at −5 mA was 65 and 45 pW while the power emitted at $I=5$ mA was 95 and 62 pW, respectively.

The dynamics were also somewhat asymmetric with respect to reversal of magnetic field, which is likely caused by a combination of the Oersted field produced by the current and device shape imperfections.[15] At negative fields, precession peaks appeared at negative current but precession was suppressed at positive current (right panels in Fig. 4). In particular, the microwave power emitted at −5 mA was 119, 176, 121, and 73 pW for $H=-200$, −400, −600, and −800 Oe, respectively. Meanwhile, the power emitted at 5 mA was only 58, 54, 45, and 44 pW for the same values of field.

We also identified a possible correlation between the frequencies at which precession peaks broaden/disappear for one polarity of current and appear for another polarity, as illustrated in Fig. 5 for $E2$ at $H=600$ Oe. Dashed line in panel (a) shows that broadening of the fundamental harmonic at negative current occurred at the same frequency as the onset of precession at positive current. The total microwave power in the first harmonic at negative current similarly rapidly decreased below the measurement noise floor, as its frequency approached the onset of precession at positive current [panel (b)].

Similar correlations are apparent in Figs. 2 and 4. In Fig. 2(e), broadening of the precession peak at negative current does not occur up to the largest measured $I=-8$ mA. How-

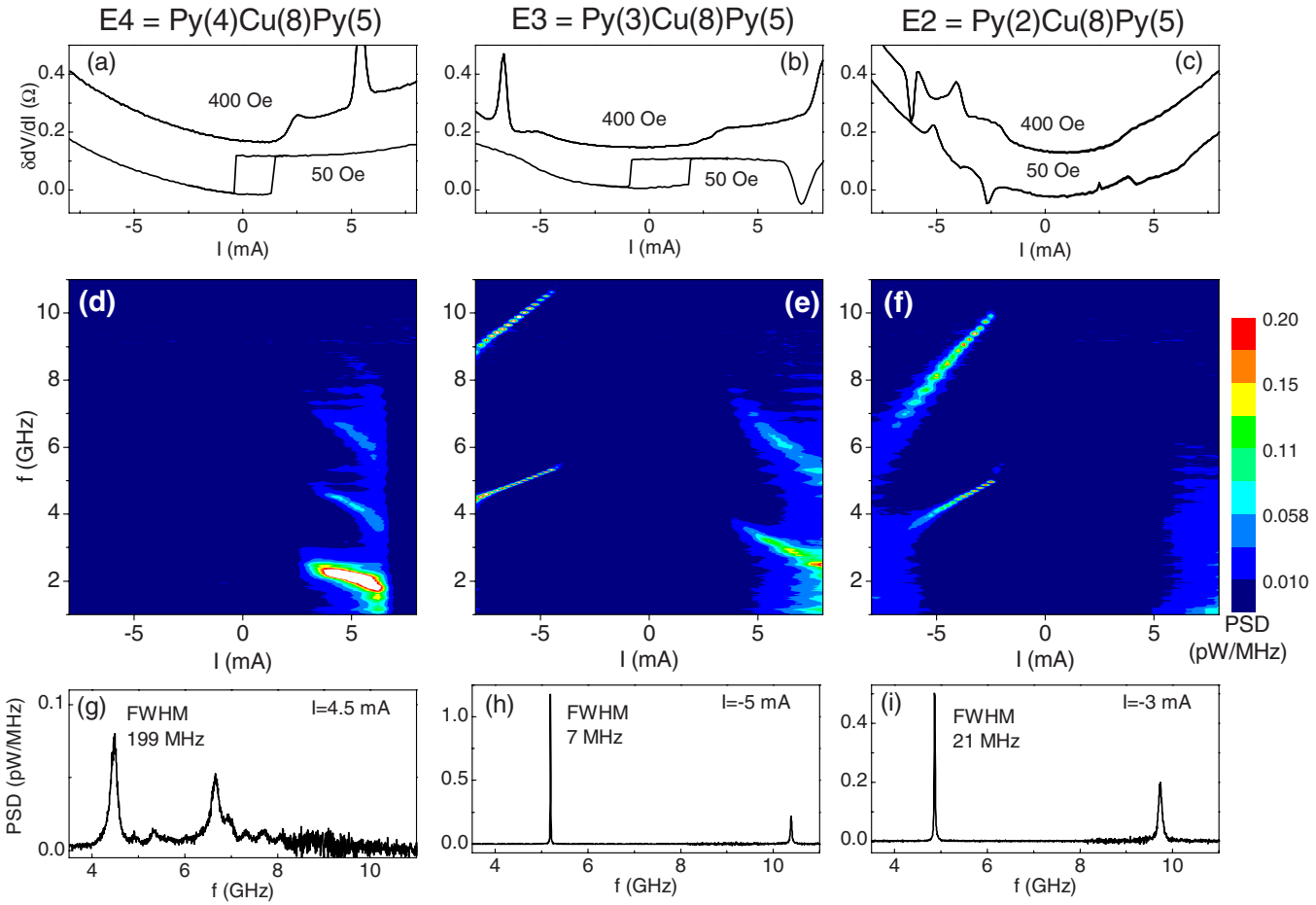

FIG. 2. (Color online) Data for devices with extended reference layer: $E4$ [(a), (d), and (g)], $E3$ [(b), (e), and (h)], and $E2$ [(c), (f), and (i)]. (a)–(c) dV/dI vs I at the labeled values of H. Curves are offset for clarity. (d)–(f) PSD at $H=400$ Oe. (g)–(i) cross sections of (d)–(f), at the labeled values of I. The peaks are harmonically related.

ever, the precession frequency $f=4.3$ GHz at this current is larger than the precession onset frequency $f=3.9$ GHz at positive current. In Fig. 2(f), abrupt broadening and reduction in precession peak occurs at $I=-5.7$ mA. The precession frequency of $f=3.7$ GHz at this current is correlated with a small broad peak apparent at $I=5.5$ mA. In Fig. 4 at $H=200$ Oe, the precession onset frequency $f=4.1$ GHz at $I=-3$ mA is correlated with the suppression of precession at $I=5.7$ mA. In this case, the precession frequency at positive current is larger than the onset at negative current. The correlation is more difficult to identify in other data for devices with extended reference layer due to the strong suppression of precession for one of the current polarities. In devices with patterned reference layer (Fig. 1), the dynamical properties of both layers are similar, making it impossible to observe the correlation.

III. MODELS

Our measurements established a correlation between the precession of reference layer at negative current and precession of the free layer at positive current, and demonstrated the dependence of the precession amplitudes on reference-layer dimensions. A theoretical treatment of these behaviors must simultaneously account for the dynamics of both layers. The two layers in our devices exhibit similar spin-polarizing properties and thus also experience a similar magnitude of STT. According to Eq. (1), positive current results in repulsion of s_F from s_R due to STT. Conversely, s_R is attracted to s_F. We are not aware of any other physical system exhibiting this type of interaction between two elements, in apparent violation of Newton's third law. However, one can show that the underlying angular momentum conservation law is satis-

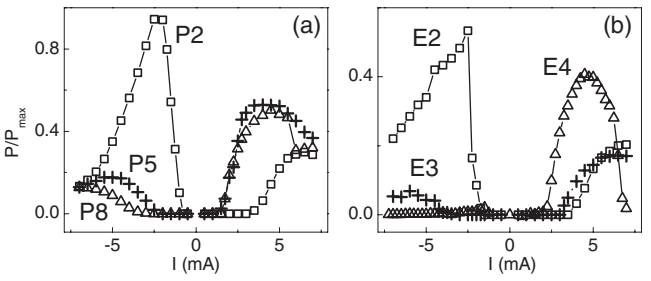

FIG. 3. Total microwave power emitted at 1–13.5 GHz normalized by the largest possible emitted power P_{max}, calculated as described in the text. (a) $P2$ (squares), $P5$ (crosses), and $P8$ (triangles). (b) $E2$ (squares), $E3$ (crosses), and $E4$ (triangles).

fied due to the spin relaxation in the magnetic layers and the leads.

The dynamical states of two magnetic moments influenced by STT can be analyzed by simultaneously solving the Landau-Lifshits-Slonczewski equations describing the magnetic dynamics in the presence of STT [Eq. (1)],[1,16]

$$\dot{\mathbf{s}}_{F,R} = \mathbf{s}_{F,R} \times \left[\gamma(\mathbf{H}_e - \alpha \mathbf{s}_{F,R} \times \mathbf{H}_e) + \frac{I g_{F,R}}{e S_{F,R}} \mathbf{s}_F \times \mathbf{s}_R \right], \quad (3)$$

where γ is the gyromagnetic ratio, $\mathbf{H}_e(s_F, s_R)$ is the effective magnetic field that includes the external field H, the demagnetizing field, and the dipolar coupling field, and α is the damping parameter. Equation (3) was solved analytically by one of us (S.U.) in the approximation of small-angle precession and negligible demagnetizing and dipolar effects.[16] This approximation implies the same precession frequency for both layers. The stationary nonstatic solution of Eq. (3) involves simultaneous correlated precession of the reference layer and the free layer with relative amplitudes determined by the inverse ratio of their total spins S_R and S_F. The onset current for the coupled precession is

$$I_c = I_{c0}/(1 - K g_R S_F / g_R S_R), \quad (4)$$

where I_{c0} is the onset current for precession of the free layer if the dynamics of the reference layer is negligible (e.g., if it is very thick), and K is a parameter of order one determined by the magnetic properties of the layers. For similar magnetic and polarizing properties of reference layer and free layer, $g_R = g_F$ and $K=1$, yielding $I_c = I_{c0}/(1 - S_F/S_R)$. The value of $I_c = I_{c0}$ for $S_R \gg S_F$ is consistent with negligible effects of STT on the reference layer; it increases with decreasing S_F/S_R and diverges at $S_F = S_R$. For $S_F > S_R$, the sign of I_C is reversed, in remarkable agreement with the observed suppression of precession at positive current, and its appearance at negative current. Analysis of stable *static* configurations shows that STT also enhances the stability of the antiparallel configuration at $I < I_c$. The broad-spectrum background for nanopatterned layers is consistent with thermal activation between the parallel state and the antiparallel state stabilized by STT.

One can define an effective volume of extended reference layer by the area somewhat larger than the point contact that experiences significant dynamics due to STT. Assuming that effectively $S_F = S_R$ for the device $E3$, all the dependences of current-induced behaviors on t_R in Fig. 2 are consistent with the above analysis and Eq. (4). However, the onset precession frequency of extended reference layer is 2 GHz higher than the frequency of a nanopatterned free layer (see Fig. 2), violating the central assumptions of the model. The higher precession frequency of the reference layer is likely caused by the exchange interaction between the point-contact area and the extended film. The model may also not be applicable to devices with nanopatterned reference layer because the neglected demagnetizing and dipolar fields have significant effects on the dynamical properties of the layers. Below, we analyze the implications of different dynamical properties of the two layers and describe numerical simulations that include the effects of demagnetizing and dipolar fields.

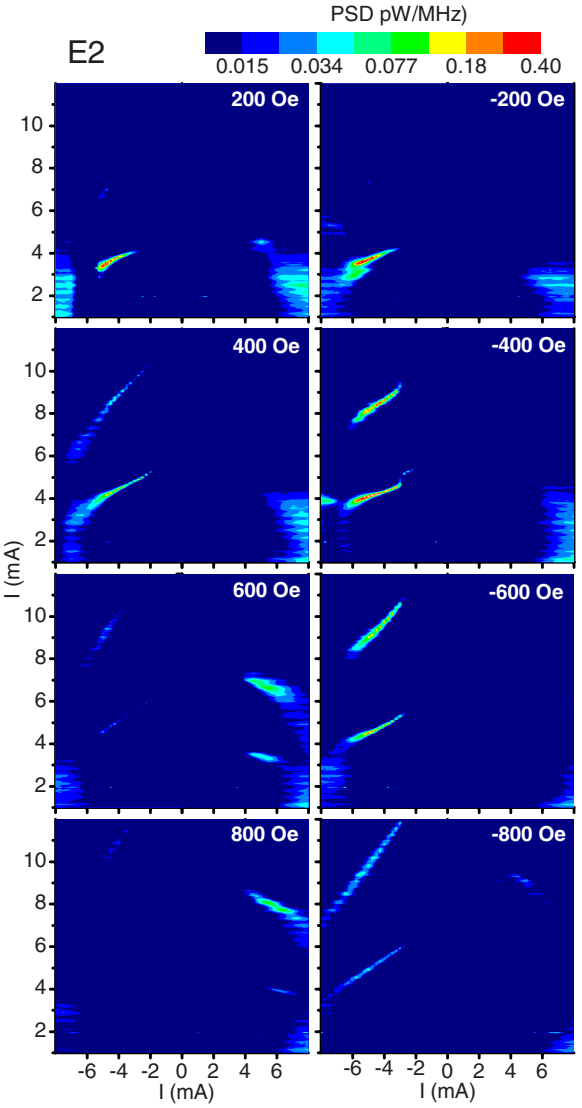

FIG. 4. (Color online) PSD vs I for sample $E2$ acquired at the labeled values of H rotated by 55° with respect to the nanopillar easy axis.

A. Analytic model

We consider a small-angle approximation for the dynamics of macrospins representing the magnetic moments of reference and free layers. For devices with extended reference layer, the point-contact area of this layer is approximately treated as a macrospin experiencing an additional effective field due to the exchange coupling to the extended film. Linearizing the Landau-Lifshits-Gilbert-Slonczewski equation [Eq. (3)] around the equilibrium orientation, which with no loss of generality can be chosen along the z axis, we obtain

$$\frac{d\xi_{R,F}}{dt} = i\omega_{R,F}\xi_{R,F} - \Gamma_{R,F}\xi_{R,F} - Ik_{R,F}(\xi_R - \xi_F). \quad (5)$$

Here, $\xi_{R,F} = s_{Rx,Fx} + i s_{Ry,Fy}$ are complex coordinates representing the projections of the macrospins on the xy plane. The first term on the right describes precession around the magnetic field, the second term describes relaxation, and the third

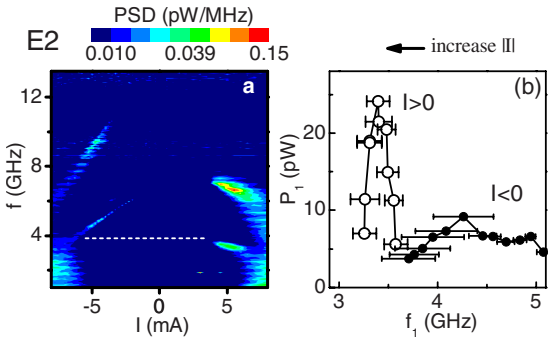

FIG. 5. (Color online) (a) PSD for $E2$ at $H=600$ Oe, rotated by 55° with respect to the nanopillar easy axis. (b) Integrated power P_1 in the first precession harmonic vs its peak frequency f_1 at negative current (solid symbols) and positive current (open symbols). Horizontal bars show FWHM. Arrow on top shows the direction of increasing $|I|$.

term describes interaction between $\mathbf{s}_R$ and $\mathbf{s}_F$ due to STT. The coefficients $\omega_{R,F}$ depend on $\xi_{R,F}$ due to the demagnetizing fields of nanomagnets. By rescaling s_{Rx}, s_{Fx}, s_{Ry}, s_{Fy}, and t, this dependence can be transferred to $\Gamma_{R,F}$ and $k_{R,F}$. Assuming that the precession term is dominant, these coefficients can be replaced with their averages over the precession cycle. Within these approximations, Eq. (5) with constant coefficients can be used to analyze the small-amplitude dynamics of the bilayer. We note that the STT term in Eq. (5) acquired an explicit form of attraction/repulsion of the points ξ_R and ξ_F representing the magnetic moments of the two layers.

Assume that $\xi_{R,F}$ precess at a common angular frequency ω, with a precession phase offset ϕ, $\xi_R=A_R e^{i\omega t}$, and $\xi_F=A_F e^{i\omega t+i\phi}$. Equation (5) then reduces to two complex algebraic relations,

$$i\omega = i\omega_{R,F} - \Gamma_{R,F} \mp Ik_{R,F}[1-(re^{i\phi})^{\pm 1}] \tag{6}$$

for the unknowns ω, ϕ, $r=A_F/A_R$, and I. The value of I determined from these relations corresponds to the onset of the current-induced precession. Assuming for simplicity $\Gamma_R=\Gamma_F$ and subtracting the two equations, we obtain $\cos\phi=(k_R+k_F)/(k_R r+k_F/r)$ from the real part and $\sin\phi=(\omega_R-\omega_F)/(Ik_F/r-Ik_R r)$ from the imaginary part. For positive current, the dynamics of the free layer may be expected to dominate so that $r\gg 1$. In this case, $\cos\phi\approx(k_R+k_F)/k_R r\ll 1$, and therefore $\sin\phi\approx -1$ for $\omega_R>\omega_F$, giving $r=(\omega_R-\omega_F)/Ik_R$. From Eq. (6), $\omega\approx\omega_F$ and $I\approx\Gamma/k_F$. Stability analysis can be performed by assuming small deviations Δr and $\Delta\phi$ of the respective variables from the stationary values determined above, and inserting them into Eq. (5). The spectrum of the resulting linear differential system lies entirely in the left half of the complex plane, confirming the stability of this dynamical state.

From the expressions for r and I above, one can see that the condition $r\gg 1$ is satisfied for similar k_R and k_F only if $|\omega_R-\omega_F|\gg\Gamma$, i.e., when the dynamical properties of the magnetic layers are sufficiently different. For $|\omega_R-\omega_F|\leq\Gamma$, the dynamics must instead involve precession of both layers with similar amplitudes, consistent with the published results.[16] Analysis similar to that given above also yields a stable dynamical state with $r\ll 1$ at negative current, as long as ω_R and ω_F are sufficiently different. In contrast, assuming $r\ll 1$ at positive current or $r\gg 1$ at negative current, we obtain a dynamical state which is not stable with respect to small perturbations of r and ϕ.

To summarize our analysis, the small-amplitude dynamical state of the bilayer depends on the dynamical properties of each layer. If the precession frequencies of the two layers are sufficiently close, both layers precess simultaneously at an onset current determined by the ratio of their magnetic moments. For different precession frequencies, precession of predominantly free layer is induced at positive current and precession of predominantly reference layer is induced at negative current, regardless of the relation between their magnetic moments. Our analysis thus supports the possibility of bipolar precession seen in "symmetric" device $E3$ and in some regimes in $E2$.

The rapid suppression of precession in "asymmetric" device $E4$ and in some regimes in $E2$, indicates that the dynamical coupling of the two layers is more robust than would be anticipated based on the different precession frequencies of the extended and the nanopatterned layers. We note that small-angle macrospin precession frequency $f\approx 8$ GHz for the free layer at $H=600$ Oe can be calculated using Kittel formula by using the magnetization $M=700$ G for Py. The lower onset frequency of ≈ 4 GHz in our data, as well as reduction in the precession frequency with increasing current is a nonlinear effect due to the growth of the oscillation amplitude.[17] Thus, free layer can behave as a nonlinear oscillator whose frequency can tune into resonance with the reference layer, suppressing precession of the latter. A similar argument can be used to explain the suppression of precession of the free layer by the dynamics of the reference layer. In the latter case, the frequency of precession of the reference layer can also vary with the precessing area of the extended film in the vicinity of the point contact.

B. Numeric calculations

The analysis described above was performed in the approximation of small-angle precession, neglecting the dipolar coupling between magnetic layers. To determine whether the dynamical coupling between ferromagnets induced by STT is robust with respect to perturbations such as dipolar coupling and nonlinear effects of large-amplitude dynamics, we also performed numeric simulations. Here, we focus only on macrospin simulations for devices with nanopatterned reference layer. The free layer was approximated by an ellipse with dimensions of 100×50 nm^2, whose demagnetizing factors were calculated analytically in the thin-ellipsoid approximation.[18] The simulated dimensions of the reference layer depended on its thickness due to the conical shape of the nanopillar. Below, we discuss results for $t_R=2$ nm and $t_R=8$ nm, with dimensions of 110×55 nm^2 and 120×60 nm^2, respectively. The dipolar coupling field for each layer was proportional to the in-plane component of the demagnetizing field for the other layer, with the coefficient of proportionality of 0.7 adjusted to reproduce our measurements of magnetoresistance vs H.

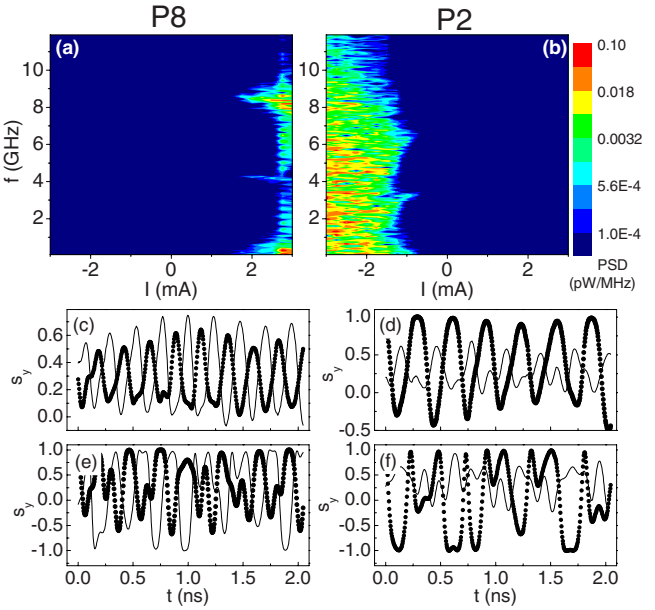

FIG. 6. (Color online) Numerical simulations of current-induced dynamics at 295 K. (a) PSD vs I for $P8$ at $H=750$ Oe rotated by 40° with respect to the nanopillar easy axis. (b) PSD vs I for $P2$ at $H=450$ Oe. (c) Time trace of in-plane hard-axis component of s_F (line) and s_R (dots) for $P8$ at $I=2$ mA. (d) same as (c) for $P2$ at −1 mA. (e) same as (c) at 4 mA and (f) same as (c) for $P2$ at −2 mA.

Simulations included the thermal fluctuations at 295 K in the form of random Langevin field. We used current polarization $p=0.5$ and saturation magnetization measured by vibrating sample magnetometry varied from 650 G for 2-nm-thick Py films to 750 G for 20-nm-thick films. We used the former value in all calculations to partially account for the dynamical inhomogeneities reducing the magnetic moment of the nanopatterned layer. The Gilbert damping constant describing ferromagnetic resonance in Py films is $\alpha=0.01$. Current-induced dynamics involves excitation of several dynamical modes simultaneously with precession, which in the macrospin approximation is taken into account by a larger value $\alpha=0.03$.[19]

The microwave spectra were calculated from the simulated time-dependent magnetization distribution of the nanopillar. The time-dependent resistance was $R(t)=R_0+\Delta R(t)$, where $R_0=(R_P+R_{AP})/2$ and $\Delta R(t)=(R_P-R_{AP})\langle \mathbf{s_R}\cdot\mathbf{s_F}\rangle/2$. The ac voltage on the input of the amplifier $V(t)=\frac{I\Delta R(t)}{1+R_0/50\ \Omega}$ was calculated by assuming that a constant current I was split between a $R_L=50\ \Omega$ load and a resistor $R(t)$ representing the sample. Fast Fourier transform of $V(t)$ over a period of $\tau=16$ ns with a 2 ps step was performed after relaxation for 8 ns. The power spectral density was determined by $\mathrm{PSD}(f)=2V^2(f)/(50\ \Omega\ \Delta f)$, where $\Delta f=1/\tau$ and a factor of 2 accounts for the negative-f contribution to the fast Fourier transform.

Figures 6(a) and 6(b) show the simulated power spectral density for $P8$ and $P2$, respectively. Current-induced precession peaks appear only at positive current for $P8$, and only at negative current for $P2$, consistently with the experimental results (Fig. 1). The simulation length of 16 ns was too short to reproduce the thermal switching of the magnetic configuration, resulting in complete suppression of excitations for the opposite polarity of current. Above the precession onset, the peaks were quickly replaced by a broad noise, consistent with our measurements. Similar noise also appeared in simulations performed at 5 K (not shown), excluding thermal fluctuations as their primary origin.

Analysis of the time traces of s_R and s_F just above the precession onset [Figs. 6(c) and 6(d)] shows that both layers precess with a similar amplitude and opposite phase. Analytical calculations neglecting the dipolar coupling yielded in-phase precession, suggesting that dipolar coupling has a significant effect on the coupled dynamics. At larger I, precession phase locking is lost due to the opposing effects of dipolar coupling and STT [Figs. 6(e) and 6(f)]. The resulting aperiodic dynamics explains the broad noise that replaced the precession peaks.

C. Effects of negative spin anisotropy

The results described above showed that current-induced precession is suppressed by simultaneous effects of STT on both magnetic layers. This effect, potentially detrimental to the performance of magnetic devices, can be minimized by optimizing the dimensions of the reference layer and enhancing its magnetic damping rate. STT-induced coupling can also enhance the effects of current in devices with inverted spin-polarizing properties of the reference layer.[16] Here, we describe a practical device architecture that utilizes this effect.

Spin-dependent scattering of electrons in Py and at its interfaces with Cu results in spin polarization in the majority direction. In contrast, scattering in FeCr alloy and at its interfaces with Cr results in minority polarization.[20] We label these two cases positive and negative spin anisotropy, respectively. The effect of negative anisotropy of the reference layer is described in Eqs. (1) and (3) by $g_R<0$. As a result, I_c is reduced relative to its value for negligible effects of STT on the reference layer. For identical magnetic properties of the two layers and $g_R=-g_F$, $I_C=I_{C0}/(1+S_F/S_R)$.[16] The reduction is caused by the mutual repulsion of s_R and s_F, resulting in their simultaneous precession with opposite phases, thus increasing the magnitude of their vector product that determines the STT in Eq. (1).

A bilayer with opposite anisotropies of two magnetic layers, proposed in Ref. 16, suffers from small magnetoresistance due to the weaker polarizing properties of the known materials and interfaces with negative spin anisotropy.[22] To simultaneously achieve a large magnetoresistance and enhance the effect of current, we propose a modified device geometry including a CoFe free layer sandwiched between a fixed bottom CoFe reference layer with positive anisotropy, and a thin FeCr reference layer with negative anisotropy on top of the free layer [Fig. 7(a)]. This structure builds on the previously proposed geometry with two fixed polarizers.[21] With an MgO tunnel barrier between the CoFe reference layer and the free layer, the resistance and the magnetoresistance of the device are almost entirely determined by this junction.

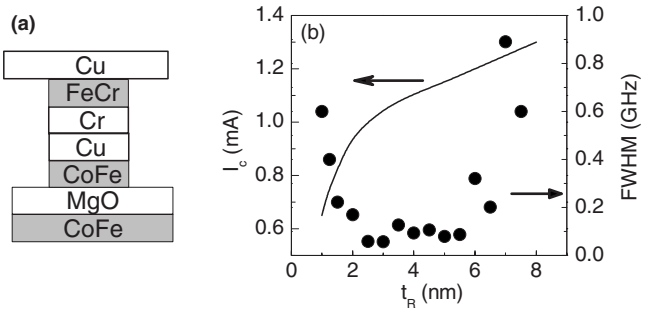

FIG. 7. (a) Structure of a device utilizing a secondary FeCr reference layer coupled by STT to the free layer to enhance current-induced switching. (b) Simulated precession onset current I_C vs the FeCr layer thickness t_R at $H=1$ kOe (solid line), and FWHM of the first precession harmonic at $H=1$ kOe, $I=1.2$ mA (dots). All calculations performed at 295 K.

The effects of current are enhanced in this architecture by two mechanisms. First, the spin currents generated by the two reference layers exert comparable STT on both interfaces of the free layer, resulting in a nearly twofold decrease in I_s even when the effects of STT on CoFe reference layer are negligible. Based on the macrospin simulations performed at $H=1$ kOe for a free layer with thickness $t_F=3$ nm and lateral dimensions of 100×50 nm^2, the precession onset is $I_C=1.5$ mA with FeCr reference layer, and $I_C=2.3$ mA without FeCr reference layer whose magnetic moment is fixed in the direction of H. Additionally, simultaneous current-induced precession of free layer and the FeCr reference layer results in reduction in the precession onset current that depends on the geometry of the FeCr layer. Here, we assume the same magnetization of 1500 G for free layer and FeCr layer, damping constant $\alpha=0.03$, the same dimensions of 100×50 nm^2 for the free layer and FeCr reference layer, and polarizing factors $p=0.9$, 0.7, and -0.5 for the CoFe, free, and FeCr layers, respectively.[22] The precession onset current I_C approaches the fixed reference layer 2 value $I_C=1.5$ mA for large t_R, and monotonically decreases for smaller t_R due to the STT-induced dynamical interaction between FeCr reference layer and the free layer [solid curve in Fig. 7(b)].

At $I=1.2$ mA, the FWHM of the first precession harmonic reaches a minimum of 57 MHz for $t_R=3$ nm. Full width at half maximum increases at larger t_R because of increasing I_C. For $t_R>6$ nm, $I_C>I$ so that the precession peak is caused by subcritical thermally activated dynamics. On the other hand, FWHM also increases for $t_R<3$ nm due to the increasing thermal fluctuations of the FeCr reference layer. The optimal device geometry can thus be determined by a compromise between the reduced precession onset current and increased linewidth for thinner FeCr reference layer.

IV. SUMMARY AND CONCLUSIONS

We presented spectroscopic measurements of current-induced magnetic dynamics in devices with similar thicknesses of the free layer and the reference layer, with the latter either left extended or patterned to the same dimensions as the free layer. Measurements for devices with a fixed thickness of the free layer and different thicknesses of the nanopatterned reference layer show that the precession of the thicker of the two layers is suppressed and replaced by $1/f$ noise attributed to random thermal switching. Devices with extended reference layer also exhibit a similar dependence on the thickness of the reference layer but the $1/f$ noise does not appear when precession of the reference layer is suppressed, which is attributed to the absence of stable antiparallel configuration in an extended magnetic film. Analytical calculations and numeric simulations suggest that the observed suppression of current-induced precession is caused by the coupling between the two layers induced by STT. We also propose a device utilizing two reference layers to enhance the effects of STT. One of the reference layers exhibits negative magnetic anisotropy. Coupling between the dynamics of this layer and the free layer results in reduction in the precession onset current.

ACKNOWLEDGMENTS

This work was supported by the NSF under Grant No. DMR-0747609 and the Cottrell Scholar award from the Research Corporation. We thank Lidiya Novozhilova for helpful discussions.

[1] J. Slonczewski, J. Magn. Magn. Mater. **159**, L1 (1996).
[2] S. S. P. Parkin, Christian Kaiser, Alex Panchula, Philip M. Rice, Brian Hughes, Mahesh Samant, and See-Hun Yang, Nature Mater. **3**, 862 (2004).
[3] S. I. Kiselev, J. C. Sankey, I. N. Krivorotov, N. C. Emley, R. J. Schoelkopf, R. A. Buhrman, and D. C. Ralph, Nature (London) **425**, 380 (2003).
[4] J. C. Sankey, I. N. Krivorotov, S. I. Kiselev, P. M. Braganca, N. C. Emley, R. A. Buhrman, and D. C. Ralph, Phys. Rev. B **72**, 224427 (2005).
[5] S. Urazhdin and N. Anthony, Phys. Rev. Lett. **99**, 046602 (2007).
[6] S. Kaka, M. R. Pufall, W. H. Rippard, T. J. Silva, S. E. Russek, and J. A. Katine, Nature (London) **437**, 389 (2005).
[7] F. B. Mancoff, N. D. Rizzo, B. N. Engel, and S. Tehrani, Nature (London) **437**, 393 (2005).
[8] S. Urazhdin and P. Tabor, J. Appl. Phys. **105**, 066105 (2009).
[9] M. Tsoi, J. Z. Sun, and S. S. P. Parkin, Phys. Rev. Lett. **93**, 036602 (2004).
[10] M. R. Pufall, W. H. Rippard, S. Kaka, S. E. Russek, T. J. Silva, J. Katine, and M. Carey, Phys. Rev. B **69**, 214409 (2004).
[11] S. Machlup, J. Appl. Phys. **25**, 341 (1954).
[12] S. Urazhdin, N. O. Birge, W. P. Pratt, Jr., and J. Bass, Phys. Rev. Lett. **91**, 146803 (2003).
[13] W. H. Rippard, M. R. Pufall, S. Kaka, T. J. Silva, and S. E. Russek, Phys. Rev. B **70**, 100406(R) (2004).

[14] G. Gerhart, E. Bankowski, G. A. Melkov, V. S. Tiberkevich, and A. N. Slavin, Phys. Rev. B **76**, 024437 (2007).
[15] W. L. Lim, A. Higgins, and S. Urazhdin, Phys. Rev. B **80**, 104408 (2009).
[16] S. Urazhdin, Phys. Rev. B **78**, 060405(R) (2008).
[17] D. V. Berkov and J. Miltat, J. Magn. Magn. Mater. **320**, 1238 (2008).
[18] R. C. Handley, *Modern Magnetic Materials, Principles and Applications* (Wiley & sons, New York 2000).
[19] G. D. Fuchs, J. C. Sankey, V. S. Pribiag, L. Qian, P. M. Braganca, A. G. F. Garcia, E. M. Ryan, Zhi-Pan Li, O. Ozatay, D. C. Ralph, and R. A. Buhrman, Appl. Phys. Lett. **91**, 062507 (2007).
[20] M. AlHajDarwish, H. Kurt, S. Urazhdin, A. Fert, R. Loloee, W. P. Pratt, Jr., and J. Bass, Phys. Rev. Lett **93**, 157203 (2004).
[21] G. D. Fuchs, I. N. Krivorotov, P. M. Braganca, N. C. Emley, A. G. F. Garcia, D. C. Ralph, and R. A. Buhrman, Appl. Phys. Lett. **86**, 152509 (2005).
[22] C. Vouille, A. Barthelemy, F. Elokan Mpondo, A. Fert, P. A. Schroeder, S. Y. Hsu, A. Reilly, and R. Loloee, Phys. Rev. B **60**, 6710 (1999).